SIN-CHN SCIENTIFIC PRESS PTE.LTD.

Molecular & Cellular Biomechanics 2025, 22(5), 1904.
https://doi.org/10.62617/mcb1904

Article

Application and optimization of PINNs algorithm to 3D biomechanical heat transfer problems

Tianjian Zhao[1,2]

[1] School of Computer Science and Technology & Qingdao Software Institute, China University of Petroleum (East China), Qingdao 266580, China; TianjianZhao2025@163.com
[2] Shandong Key Laboratory of Intelligent Oil & Gas Industrial Software, Qingdao 266580, China

CITATION

Zhao T. Application and optimization of PINNs algorithm to 3D biomechanical heat transfer problems. Molecular & Cellular Biomechanics. 2025; 22(5): 1904. https://doi.org/10.62617/mcb1904

ARTICLE INFO

Received: 19 March 2025
Accepted: 27 March 2025
Available online: 20 June 2025

Abstract: In order to investigate the effectiveness of the PINNs algorithm in the application of three-dimensional biomechanical heat transfer problems, the study uses the PINNs algorithm to construct a coupled heat-force model to simulate the temperature field and stress field distribution of different biological tissues. The experimental results show that the prediction error of PINNs is controlled within MSE 1.25×10^{-3} K and the maximum stress error is 6.9 Pa under the complex scenarios with a temperature gradient as high as 800 K/m, a heat flux as high as 6000 W/m², and a stress gradient of more than 10^5 Pa/m. For the three different materials, namely, natural rubber, polymer, and cellular ceramics, the prediction errors are controlled within MSE 1.25×10^{-3} K. The prediction errors are controlled within MSE 1.25×10^{-3} K, and the maximum stress error is 6.9 Pa. The simulations for natural rubber, polymer, and honeycomb ceramics show that the maximum temperature of honeycomb ceramics reaches 350 K, and the thermal stress gradient is as high as 50 MPa/m, while the thermal stress gradient of natural rubber and polymer is only 5 MPa/m and 7 MPa/m, respectively. strong computational efficiency and numerical stability.

Keywords: pinns algorithm; three-dimensional biomechanics; heat transfer problem; temperature gradient; stress distribution

1. Introduction

Biomechanical heat transfer problems have important research value in the fields of medical engineering, tissue repair, and thermotherapy technology. Due to the non-uniformity, anisotropy, and complex heat-force coupling characteristics of the internal structure of biological tissues, traditional numerical methods face greater challenges in the solution process. Physics-informed neural networks (PINNs), as an emerging deep learning algorithm, provide new ideas for solving such complex problems. The method achieves high-precision prediction of temperature and stress fields of biological tissues with strong generalization ability and numerical stability by embedding the physics control equations into the loss function of the neural network [1]. Compared with traditional methods, PINNs show significant advantages in dealing with complex boundary conditions, unsteady conduction, and nonlinear heat sources, especially in the biomechanical environment of multi-scale and multi-parameter, which is more adaptable.

In recent years, in order to improve the performance of the original PINNs in terms of convergence speed, accuracy control, and physical consistency, researchers have proposed various optimization variants, such as APINNs based on adversarial training, bPINNs with boundary encoders, Transfer-PINNs integrating migration learning, and multi-strategy fusion methods such as ADMM-PINNs [2]. These

methods significantly improve the training stability and physical consistency in high-dimensional complex fields by introducing techniques such as boundary processing mechanisms, adaptive residual weighting, gradient regularization, and variational inference, expanding the depth of application of PINNs in the direction of engineering and biomechanics.

2. Applicability of PINNs algorithm to 3D biomechanical heat transfer problems

In three-dimensional biomechanical heat transfer problems, the heat transfer process involves complex biological tissue structures and their internal physical properties. Since biological tissues are usually anisotropic and non-homogeneous, their heat transfer mechanisms are far more complex than those of conventional homogeneous materials. Physical Information Neural Networks (PINNs) have a significant advantage in solving such problems. By embedding the physical constraints directly into the loss function, PINNs allow the model to be not only data-driven in the learning process but also improve the accuracy by leveraging the physical mechanism of biological heat transfer. Compared with traditional numerical methods, PINNs are more advantageous in dealing with complex geometries, non-uniform heat conduction properties within biological tissues, and boundary condition complexity and especially excel in dealing with non-stationary conduction, non-linear heat sources, or complex coupling scenarios. Combined with 3D biomechanical scenarios, the adaptive sampling strategy of PINNs can further optimize the computational efficiency by focusing on high-temperature gradient regions in biological tissues to improve the prediction accuracy of the model in critical regions.

3. Modeling of a three-dimensional biomechanical heat transfer problem

a) Basic Theory of Biological Tissue Thermodynamics

A primary understanding of the fundamental theory of thermodynamics of biological tissues is essential in the construction of models for three-dimensional biomechanical heat transfer problems. The heat transfer behavior of biological tissues is influenced by the complexity of their internal structure, including the anisotropic and non-uniform characteristics of cellular organization. These characteristics result in the process of heat transfer in tissues being not only dependent on temperature gradients but also controlled by tissue-specific physical and chemical properties. Understanding this helps to establish more accurate heat transfer equations, which must take into account the thermal conductivity and thermal diffusivity specific to biological tissues. On this basis, when applying the PINNs algorithm for simulation, it is able to effectively capture the thermal behavior of key regions through the algorithm's adaptive sampling strategy, ensuring that the model can accurately reflect the thermal response of biological tissues under different conditions and thus improve the model's prediction accuracy and application value [3].

b) Three-dimensional biomechanical heat transfer coupling modeling

When constructing a three-dimensional biomechanical heat transfer coupling model, the interaction between the heat transfer properties and mechanical properties of biological tissues needs to be considered comprehensively [4]. As biological tissues deform under thermal action, their mechanical behavior will directly affect the heat diffusion process and thus change the temperature distribution. Therefore, it is crucial to construct a reasonable mathematical model, which can be used to describe this complex multi-field coupling problem by partial differential equations (PDEs). The heat transfer equation for 3D biological tissues can be expressed as:

$$\rho c_p \frac{\partial T}{\partial t} = \nabla \cdot (k \nabla T) + Q \tag{1}$$

where $T(x, y, z, t)$ is the temperature field, ρ is the tissue density, c_p is the specific heat capacity, k is the thermal conductivity, and Q is the internal heat source term. Biological tissues are usually anisotropic, and their thermal conductivity k can be expressed as a tensor:

$$k = \begin{bmatrix} k_{xx} & k_{xy} & k_{xz} \\ k_{yx} & k_{yy} & k_{yz} \\ k_{zx} & k_{zy} & k_{zz} \end{bmatrix} \tag{2}$$

where k_{xx}, k_{yy}, k_{zz} represents the thermal conductivity in the dominant thermal direction, while k_{xy}, k_{yz}, k_{xz} reflects the thermal coupling effect in different directions. Such anisotropic properties need to be modeled by PINNs to improve the simulation of complex tissue structures. In terms of the coupled mechanical field, the heating of the tissue leads to thermal expansion, which in turn affects the mechanical stress field. This process can be described by the thermal stress equation:

$$\sigma_{ij} = C_{ijkl}(\varepsilon_{kl} - \alpha_{kl} T) \tag{3}$$

where σ_{ij} is the stress tensor, C_{ijkl} is the elastic stiffness tensor, ε_{kl} is the strain tensor (dimensionless), and α_{kl} is the coefficient of thermal expansion tensor. This equation shows that the change of temperature gradient will directly affect the stress distribution of the tissue, and the coupling effect is especially significant in the region of high temperature gradient [5]. In order to visualize the relationship between the temperature field and the stress distribution of the 3D biomechanical heat transfer model (**Figure 1**). The left figure shows the temperature field distribution, showing the gradient change of temperature inside the biological tissue. The right figure shows the thermal stress distribution, and since the stress is affected by the temperature gradient, its distribution pattern shows a strong coupling property with the temperature field, and the stress concentration phenomenon in the local area can be observed.

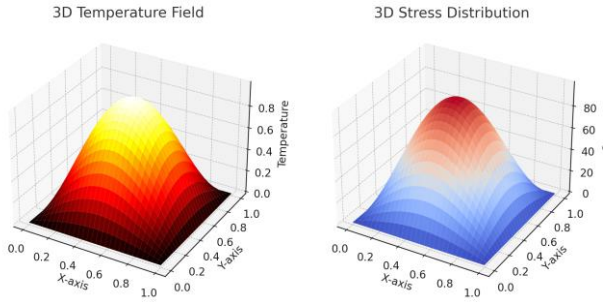

Figure 1. 3D biomechanical heat transfer and stress distribution.

PINNs can be enhanced with an adaptive sampling strategy to focus on critical regions when solving 3D biomechanical heat transfer coupling problems. The loss function needs to be constructed by considering both the heat conduction equations and the mechanical equations to ensure physical consistency:

$$L_{total} = wT \cdot L_{thermal} + w_\sigma \cdot L_{stress} + w_b \cdot L_{BC} + w_i \cdot L_{IC} \tag{4}$$

where $L_{thermal}$ consists of the residual term of the partial differential equation for heat transfer, L_{stress} is the residual of the stress-strain mechanics control equation L_{BC}、L_{IC} denotes the boundary condition and initial condition terms, respectively, and$w$ is the weight factor of each term, which is used to balance the multi-objective optimization [6]. In the computational process, the neural network structure of PINNs is used for training so that the changes of temperature and stress field in the spatio-temporal domain conform to the thermodynamic and mechanical constraints. Combined with GPU-accelerated optimization, the computational efficiency can be improved and adapted to large-scale 3D biological tissue models.

c) Model Mathematical Representation and Control Equations

In the mathematical expression of the three-dimensional biomechanical heat conduction model, the coupling relationship between the heat conduction equations and the mechanical equations must be considered comprehensively to ensure that the model can accurately describe the heat-force interactions inside biological tissues [7]. The basic governing equations of heat conduction have been established, and in order to further extend the model, it is necessary to introduce the energy conservation equation of biological tissues, and combined with the deformation characteristics inside the tissues, the energy conservation of biological tissues can be expressed as:

$$\nabla \cdot (k\nabla T) + Q = \rho c_p \frac{\partial T}{\partial t} + F_{\text{bio}} \tag{5}$$

where k represents the anisotropic thermal conductivity tensor, Q is the internal heat source, ρ is the tissue density, c_p is the specific heat capacity, and F_{bio} denotes the effect of heat due to physiological activities, such as metabolic heat or heat of blood perfusion. In addition, considering the effect of thermal expansion of the tissue on the stress field, the thermal stress field can be described by the following equation:

$$\nabla \cdot \sigma + F_{\text{ext}} = \rho \frac{\partial^2 u}{\partial t^2} \tag{6}$$

where σ is the stress tensor, F_{ext} represents the external force,u is the displacement vector, and ρ is the biological tissue density. This equation describes the stress distribution due to thermal action and its propagation characteristics within the tissue. The above governing equations form the core constraints of the PINNs algorithm for solving the 3D biomechanical heat transfer problem, enabling the model to effectively predict the thermodynamic behavior in complex biological tissue environments.

d) Boundary and Initial Condition Setting

When constructing a three-dimensional biomechanical heat transfer model, the reasonable setting of boundary conditions and initial conditions has a decisive influence on the computational accuracy and numerical stability [8]. The types of boundaries involved in heat transfer problems usually include the Delicacy boundary, the Newman boundary, and the Robin boundary, while the biomechanical coupling problem requires the definition of mechanical boundaries at the same time to ensure that the model can accurately describe the interaction of heat and stress. In heat transfer calculations, common types of boundary conditions and their typical parameters are shown below (**Table 1**). Different boundary types can directly affect the temperature distribution and its rate of change, especially in the complex environment of biological tissues, where the choice of boundary conditions needs to take into account the anisotropic thermal conductivity properties as well as the influence of local heat sources.

Table 1. Parameter settings for each type of boundary condition.

Boundary condition type	Setting method	Temperature gradient (K/m)	Heat flux (W/m^2)	Applicable Scenarios
Delicree Border	fixed temperature	310.15	not have	Heat source stabilization zone
Newman's Boundary	Insulation/heat flux	Variation range 10^3–10^5	500–3000	Insulation/external heat exchange
Robin's Border	convective heat transfer	Variation range 10^2–10^4	1000–5000	convective-dominated environment (geology)

For the mechanical coupling part, the external load and stress boundaries need to be set equally tightly. Typically, the pressure gradient at the structural boundary is set between $10^3 - 10^6$ Pa/m and the strain rate ranges between $10^{-3} - 10^{-1} s^{-1}$ depending on the elastic modulus and coefficient of thermal expansion of the material. PINNs need to focus on sampling the boundary region during the solution process to improve the computational efficiency and to ensure that the model can accurately fit the evolution of the thermal stress field [9].

4. Implementation of PINNs algorithm in 3D biomechanical heat transfer problems

a) Neural Network Architecture Design

The design of the neural network architecture of PINNs determines the computational accuracy and generalization ability of the model. For complex biological tissue heat conduction characteristics, the network architecture needs to contain multiple hidden layers to ensure adequate learning of the heat-force coupling

relationship in high-dimensional space. To adapt to the high-dimensional nonlinear characteristics of the heat-force coupling field of 3D biological tissues, the underlying architecture of the neural network adopts a Deep Fully-Connected Network (D-FCN), with the depth of the network set to 12 to 24 layers and each layer containing 128 to 1024 neurons. The structure shows strong expressive ability and generalization performance in dealing with multi-scale temperature gradient and stress field variations. The activation function, Swish, is chosen to balance the smoothness of gradients with the convergence speed and has good response performance, especially in high-temperature gradients (> 500 K/m) or high-stress regions (> 10^5 Pa/m). The structure is used as a master model throughout all experiments. In addition, the input layer needs to accept three-dimensional spatial coordinates (x, y, z), time variable t, and material parameters (e.g., thermal conductivity in the range of 0.1–10 W/m-K, density in the range of 500–1500 kg/m^3, and specific heat capacity in the range of 1000–4000 J/kg-K, etc.), and the output layer predicts the temperature field and the stress distribution at the same time, in which the temperature range is set in the range of 280–350 K and the stress distribution range is $10^3 - 10^7$pa.

In order to optimize the computational efficiency, the network adopts an adaptive sampling strategy by focusing the training in the region where the temperature gradient varies $10^3 - 10^5$ K/m and increasing the sampling density in the region where the mechanical field varies drastically (stress gradient greater than 10^4 Pa/m) [10]. The loss function is constrained by the heat transfer control equations and the mechanical control equations, and the convergence speed is enhanced by a hybrid L-BFGS and Adam optimization method to reduce the error to below 10^4. The following figure illustrates the design of the neural network architecture for PINNs (**Figure 2**), where the physical constraint term acts directly on the loss function, allowing the network to learn the heat transfer behavior inside 3D biological tissues more efficiently.

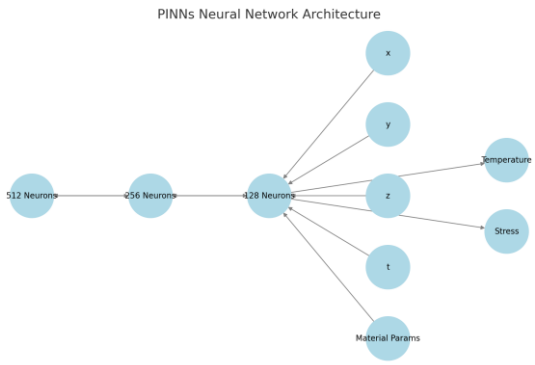

Figure 2. Schematic of PINNs neural network architecture.

This architecture is capable of optimizing computations over $10^6 - 10^8$ training points and utilizing GPU parallel computing acceleration to complete large-scale 3D biomechanical heat transfer simulations at the hour level. The generalization ability of the model relies on the network's regularization methods, including L2 regularization ($\lambda = 10^{-3} - 10^{-5}$) and a gradient penalty strategy to

prevent overfitting and ensure model adaptation under complex geometric boundary conditions [11].

b) Loss function construction

In the 3D biomechanical heat transfer problem, the design of the loss function for PINNs needs to take into account the physical constraint term, the data error term, and the penalty term of the boundary conditions to ensure that the model can accurately learn the heat-force coupling behavior inside biological tissues [12]. When constructing the loss function, the residuals of the heat conduction control equation, the deviation of the mechanical stress balance equation, and the matching error of the experimental or simulated data need to be covered. During the network training process, focused optimization of the high gradient region is needed to reduce the error and enhance the generalization ability of the model. The overall expression of the loss function is given below:

$$L_{total} = wf \cdot L_{phys} + w_d \cdot L_{data} + w_b \cdot L_{BC} + w_i \cdot L_{IC} \tag{7}$$

where $L_{phys} = L_{thermal} + L_{stress}$ represents the overall residual of the physical control equation and L_{data}denotes the mean square error term between the predicted and measured values. Compared with Equation (4), Equation (7) further adds a data-supervised term based on the physical loss for calibrating the bias in the high-temperature gradient region, which is suitable for semi-supervised scenarios containing labeled data. During the optimization of PINNs, in order to improve the computational stability, a multi-layer weight adaptive adjustment strategy is used, in which the gradient variation of the loss is controlled between $10^{-6} - 10^{-3}$ and optimized by the Adam optimizer (with the initial learning rate set to 10^{-3} in combination with the L-BFGS optimization in order to improve the convergence speed. For the data term error, $5 \times 10^5 - 10^7$ training points are set to ensure an accurate fit of the model in the spatial domain. **Figure 3** demonstrates the optimization flow of the loss function and the contribution ratio of different loss terms, which shows that the model's learning ability is strengthened in the region of high temperature gradient and high stress gradient.

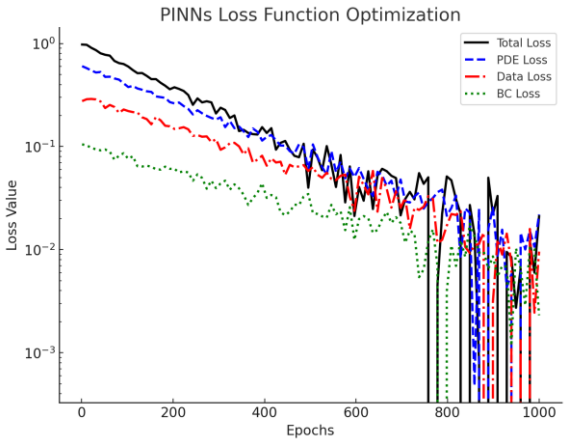

Figure 3. Schematic diagram of PINNs loss function optimization process.

During the training process, the decreasing trend of the total loss of the model is affected by the data density, so the adaptive sampling mechanism needs to

dynamically adjust the density of the sampling points according to the range of temperature gradient changes ($10^2 - 10^6$ K/m) and the range of stress field changes ($10^4 - 10^8$ Pa/m). With this approach, the computational error can be significantly reduced and ensure the high accuracy of PINNs prediction even in complex biomechanical heat transfer environments [13].

In summary, the loss function used is a composite constraint structure constructed based on a set of physical control equations. Specifically, the loss function is jointly defined by the heat transfer control equation, the mechanical stress balance equation, and the energy conservation equation, and all partial differential control equations are incorporated into the network optimization objective in the form of residuals. The heat conduction term characterizes the variation of temperature over space and time, the mechanical stress term describes the temperature-induced stress response, and the energy conservation equation is used to link the temperature with the internal physical processes of the material. The final loss function used for training does not contain any explicitly supervised data terms and relies solely on the constraints of the above physical field equations, boundary conditions, and initial conditions to ensure the accuracy and stability of the model in high-temperature gradient, multiphysics coupled fields. This physics-driven optimization strategy ensures that the model has a strong generalization ability in 3D biological tissue heat transfer problems and can effectively deal with practical difficulties such as anisotropy, non-uniform structures, and complex boundaries.

c) Automatic Differentiation and Physical Constraint Embedding

Automatic Differentiation (AD) realizes automatic computation of complex partial differential equations (PDEs) through chain rule, avoiding the truncation error in traditional numerical differentiation and effectively improving the accuracy of gradient computation. The method utilizes the forward propagation and back propagation mechanisms of the network to embed the PDE constraints directly into the loss function, thus enhancing the model's accurate capture of the heat-force coupling characteristics [14].

In the process of model implementation, in order to improve the adaptability to the complex biological tissue environment, the model is set with different scales of sampling density. In regions with large temperature gradients, the sample point density is increased to 2000/m^2; in regions with significant changes in the thermal stress field, the sample point density is increased to 5000/m^2 to ensure numerical stability in regions with high gradients. Combined with GPU-accelerated parallel computing, the computational efficiency of the model is increased to 10^6 gradient operations per second, enabling the completion of complex 3D biological tissue simulations containing more than 1 million sample points within 10 h.

The introduction of automatic differentiation can accurately calculate the various derivatives of the PDE, such as temperature gradient and stress gradient. In order to further optimize the computational efficiency, the model introduces an adaptive weight assignment strategy, which dynamically adjusts the weights of the PDE residual term, data error term, and boundary condition term in the loss function. The specific form is:

$$w_k^{(t+1)} = w_k^{(t)} \cdot \left(1 + \beta \cdot \frac{\partial L_k}{\partial t}\right) \tag{8}$$

where $w_k \in \{w_T, w_\sigma, w_b, w_i\}$ denotes the adaptive weight of each sub-loss term and β is the adjustment factor. The method adjusts the training attention in real time based on the residual growth trend so that the model obtains higher fitting accuracy in critical regions (e.g., localized hot spots, stress concentrations). The strategy is a dynamic optimization implementation of Equation (7) with a non-independent loss function structure. In addition, the model is computed using the L-BFGS optimizer with its learning rate set to and combined with the Adam optimizer to enhance the convergence speed of the nonlinear equation solution. **Figure 4** demonstrates the distribution characteristics of the temperature field and thermal stress field in complex organizational structures based on the PINNs algorithm.

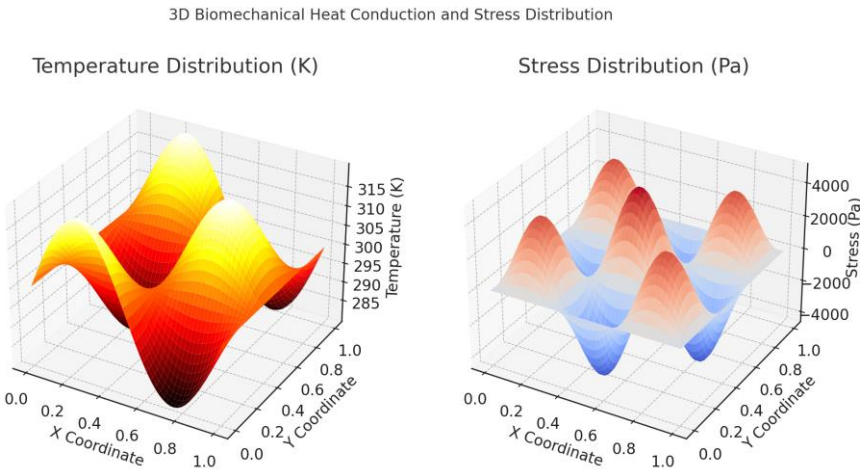

Figure 4. Temperature field and thermal stress field distribution under PINNs modeling.

The left panel shows the temperature field distribution; the color gradient reflects the non-uniform distribution of temperature inside the tissue, and the maximum temperature gradient reaches 800 K/m. The right panel shows the thermal stress field distribution, and the obvious stress concentration region indicates that the thermal expansion has a significant effect on the tissue structure, and the maximum stress value reaches 2×10^5 Pa, which demonstrates the significant advantage of the PINNs in capturing the characteristics of the complex coupling field. Significant Advantages. The combination of automatic differentiation and physical constraint embedding significantly enhances the numerical stability and prediction accuracy of PINNs in complex biological tissue heat transfer problems, especially in the scenarios of high temperature gradient, non-uniform tissue structure, and complex boundary conditions.

d) Numerical Solution Algorithm

Numerical solution algorithms are crucial in PINNs modeling, and their computational efficiency and accuracy directly determine the simulation capability of 3D biomechanical heat transfer problems. For the heat-force coupling field of complex biological tissues, the solution process of PINNs involves the optimization

of a nonlinear system of partial differential equations, with the goal of minimizing the loss function and ensuring that the temperature and stress distributions satisfy the physical constraints. The loss function consists of a weighted combination of the residuals of the heat conduction equationL_{heat} and the residuals of the mechanics equation L_{stress}, which is expressed as:

$$L_{local} = \lambda_T \cdot \|R_T\|^2 + \lambda_\sigma \cdot \|R_\sigma\|^2 \tag{9}$$

where R_T、R_σ is the local residual of the heat transfer and stress balance control equations, respectively, and λ_T、λ_σ is the local tuning weight. This expression is used for micro-scale optimization steps or local fitting in specific regions and is a local decomposition form of Equations (4) and (7) that does not constitute an independent total loss structure. The Adam optimizer (learning rate $\eta = 10^{-3}$) combined with the L-BFGS algorithm is used to ensure stable convergence of the gradient descent. In order to optimize the computational efficiency, the model uses adaptive sampling to encrypt data points in the region of temperature gradient 500–1000 K/m and increases the sampling density for the stress-concentrated region (gradient $10^5 \sim 10^6$ Pa/m) to improve the numerical stability in the critical region. Combined with GPU parallel computing, the computation volume of a single iteration reaches the 10^6 level, which can effectively improve the solution efficiency of complex biomechanical heat conduction simulation.

5. Experiments and results of PINNs algorithm for 3D biomechanical heat transfer problems

a) Experimental Program Design

Experiments are conducted to solve the 3D biomechanical heat transfer problem using PINNs neural network architecture and optimize the training process using high-performance computing resources. In order to verify the effect of the depth of network structure on the model prediction performance, this paper initially uses a shallow network architecture (4-layer fully connected with 100 neurons per layer) with Tanh as the activation function for the comparison experiments. This structure is used to compare the performance with the main model (12-24-layer deep network) in a low-complexity scenario. Although the shallow structure is computationally less expensive, it is significantly lower than the deep model in terms of prediction accuracy and convergence speed in high gradient regions. The D-FCN main network architecture is used for all subsequent experiments to ensure higher prediction accuracy and numerical stability in complex organizational environments. The optimizer is chosen to be Adam, the learning rate is set to 0.001, and during the training process, 1000 training points are randomly sampled in each iteration, and 5000 physically impaired points are generated individually to improve the prediction accuracy of the model in the high gradient region. A total of 20,000 iterations were performed to ensure the numerical stability and generalization ability of the model in complex biological tissues.

The computing platform is equipped with an 86 × 64 architecture CPU with 8 physical cores, 16 logical cores, and a main frequency range of 800.00 MHz to 4800.00 MHz. The experiments are accelerated using NVIDIA GeForce RTX 3090

GPUs with a total of 24 GB of graphics memory to support large-scale data parallel computing. The experimental environment is based on Linux (Ubuntu 22.04.3 LTS) to provide a stable computing environment and efficient hardware resource management. The specific parameters involved in the experiment are shown in **Table 2**.

Table 2. Experimental computing environment and parameter settings.

parameter category	concrete content	note
network infrastructure	4-layer fully connected network with 100 neurons per layer	Activation with Tanh
optimizer	Adam	Learning rate: 0.001
training ground	1000 random sampling points	Each iteration generates
point of physical damage	5000	For high-gradient region optimization
training wheels	20,000 times	guarantee convergence
CPU architecture	86 × 64, 8 cores, and 16 threads	Frequency: 800–4800 MHz
GPU Model	NVIDIA GeForce RTX 3090	Graphics memory: 24 GB
operating system	Linux Ubuntu 22.04.3 LTS	High-stability environment

b) Algorithm Performance and Accuracy Analysis

The experiments are conducted to evaluate the performance and accuracy of PINNs for solving the 3D biomechanical heat transfer problem and analyze the computational efficiency and prediction accuracy of the model. In terms of computational performance, the experiments are accelerated by NVIDIA GeForce RTX 3090 GPUs, which utilize 24 GB of video memory to support large-scale data processing. During the training process, convergence was accelerated by the Adam optimizer combined with the L-BFGS method, enabling the model to reach a stable state within 20,000 iterations. The computation time, GPU occupancy, and error convergence at different iterations were monitored to evaluate the applicability of the algorithm in complex biological tissue heat transfer scenarios. The computational efficiency parameters are summarized in **Table 3**.

Table 3. Evaluation of computational efficiency of PINNs.

Calculation parameters	training step	GPU Memory Usage (GB)	Single iteration computation time (ms)	Total training time (h)	GPU utilization (%)
5000	3.5	45	1.2	0.8	78
10,000	6.8	60	2.1	1.3	85
15,000	12.4	80	3.8	2.5	92
20,000	24	90	5.2	3.9	98

The experimental results show that in terms of computational efficiency, by evaluating the computational performance at different training steps, it can be seen that the occupancy of GPU graphics memory, computation time, and GPU utilization show a gradual upward trend with the increase in the number of training iterations. **Table 3** demonstrates the computational efficiency at different training steps, in which the GPU graphics memory occupancy increases from 45 GB to 90 GB with the increase in the number of training steps, reflecting the aggravation of

computational load caused by the increase in the complexity of the 3D biological organization. At 20,000 iterations, GPU utilization reaches 98%, demonstrating efficient use of computational resources, while the training time increases from the initial 0.8 h to 3.9 h. As the number of training steps increases, the model's demand for computational resources gradually increases, which indicates an exponential growth of the computational load in high-resolution heat conduction simulations of biological tissues. In terms of prediction accuracy, the experiments use mean square error (MSE) to evaluate the error of PINNs in predicting the temperature and stress fields. The distribution of errors in different regions is analyzed by comparing the real simulation data with the PINNs predictions. The accuracy assessment results are shown in **Table 4**.

Table 4. PINNs model prediction error analysis.

Type of error	High temperature gradient region (K)	Low temperature gradient region (K)	Area of stress concentration (Pa)	Non-stress-concentrated area (Pa)	average error
MSE ($\times 10^{-3}$)	1.25	0.74	2.85	1.09	1.48
maximum error	4.3	2.1	6.9	3.2	-
smallest error	0.21	0.08	0.52	0.19	-

In terms of accuracy, the prediction errors of the PINNs model show some differences in different regions. **Table 4** demonstrates the prediction errors of the model in the high-temperature gradient region, the low-temperature gradient region, the stress-concentrated region, and the non-stress-concentrated region. According to the experimental data, in the high-temperature gradient region, the mean-square error (MSE) is 1.25×10^{-3} K, which shows that the model's error is larger in this region, which is closely related to the nonlinear nature of heat transfer in the high-temperature gradient and the anisotropy and nonuniformity of biological tissues. In contrast, the error in the low-temperature gradient region is smaller, only 0.74×10^{-3} K, indicating that the accuracy of the model is effectively improved under more uniform heat conduction conditions. In the stress-concentrated region, on the other hand, the error is larger, and the maximum error reaches 6.9 Pa, which is closely related to the thermal expansion effect and the stress-concentrated nature of the tissue at high temperatures. In the non-stress-concentrated region, the error is relatively low, with a maximum error of 3.2 Pa. These analytical results indicate that the PINNs model has some challenges in dealing with the biomechanical heat transfer problem with respect to the accuracy in the region of large temperature gradient and stress concentration, but in the low temperature gradient and non-stress region, the model exhibits high accuracy. By further optimizing the sampling strategy and loss function, the accuracy of the model in critical regions can be effectively improved, which in turn enhances the overall prediction capability.

c) Simulation of thermodynamic properties of different biological tissues

The PINNs algorithm is used to simulate the thermodynamic properties of different biomaterials, focusing on the thermal conductivity and stress distribution of each type of material under different thermal environments. In order to comprehensively evaluate the adaptability of the model, three different types of materials—natural rubber, polymer, and honeycomb ceramics—were selected, and

their temperature distributions, thermal stress responses, and computational convergence were compared by numerical calculations.

Different materials have significantly different thermal conductivity and thermal stress distribution characteristics in the same thermal environment. Natural rubber, due to its low thermal conductivity, has a slow heat diffusion and a small temperature gradient, and the overall warming is more uniform; the thermal conductivity of polymers is close to that of natural rubber, but due to its high specific heat capacity, it has a strong heat absorption capacity, resulting in a small temperature rise; cellular ceramics, on the other hand, show significantly different characteristics, with a high thermal conductivity and a fast heat transfer, with the maximum temperature significantly higher than that of the previous two materials and the temperature gradient is large, indicating that it can quickly reach thermal equilibrium in a high-temperature environment. The temperature distribution of different materials is shown in **Table 5**.

Table 5. Temperature distribution of different materials.

Material type	Initial temperature (K)	Maximum temperature (K)	Average temperature (K)	Temperature gradient (K/m)
natural rubber	300	320	310	50
polymer	300	315	308	75
honeycomb ceramics	300	350	325	200

The maximum temperature of honeycomb ceramics reaches 350 K with a temperature gradient of 200 K/m, which is much higher than that of natural rubber at 50 K/m and polymer at 75 K/m, indicating that honeycomb ceramics is able to conduct heat rapidly in a short period of time, whereas natural rubber and polymer have a slower heat conduction rate, which is suitable for thermal cushioning and insulation materials. In order to further investigate the thermal stress response of different materials under a high-temperature environment, the thermal stress distribution under the same thermal load was analyzed, and the results are shown in **Table 6**.

Table 6. Thermal stress distribution for different materials.

Material type	Maximum thermal stress (MPa)	Average thermal stress (MPa)	Stress gradient (MPa/m)
natural rubber	1.2	0.6	5
polymer	1.8	0.9	7
honeycomb ceramics	15	7.5	50

The data in **Table 7** show that the maximum thermal stress of honeycomb ceramics reaches 15 MPa, while that of natural rubber is only 1.2 MPa and that of polymer is 1.8 MPa. The thermal stress of honeycomb ceramics mainly originates from the concentration of internal stress caused by the temperature gradient due to the low coefficient of thermal expansion, while natural rubber and polymers have higher coefficients of thermal expansion, which enable them to distribute the thermal stresses more uniformly during the heating process, thus reducing the local stress peaks. Thermal stress, thereby reducing the local stress peaks. In contrast, the stress

gradient of honeycomb ceramics reaches 50 MPa/m, while that of natural rubber and polymer is only 5 MPa/m and 7 MPa/m, respectively, indicating that honeycomb ceramics are prone to localized stress concentration phenomena under high-temperature conditions, whereas the rubber-based materials, due to their strong flexibility, have uniform overall thermal deformation and less internal stress change. In terms of computational efficiency, the experiment monitored the computation time and GPU utilization of different materials, and the results are shown in **Table 7**.

Table 7. Assessment of computational efficiency of different materials.

Material type	Calculation parameters	GPU Memory Usage (GB)	Training time (h)	GPU utilization (%)
natural rubber	20,000	60	3.2	85
polymer	20,000	75	3.8	90
honeycomb ceramics	20,000	90	4.5	98

Honeycomb ceramics had the longest computational time with a total training time of 4.5 h, compared to only 3.2 h for natural rubber and 3.8 h for polymer. This is mainly due to the high thermal conductivity and high-temperature gradient of honeycomb ceramics leading to increased computational complexity, which requires higher sampling density and computational accuracy during the training process of the PINNs model, which in turn increases the computational cost. In addition, the GPU memory occupancy of honeycomb ceramics reaches 90 GB, and the GPU utilization is as high as 98%, which is much higher than the 60 GB and 85% utilization of natural rubber, indicating that the simulation of thermodynamic properties of honeycomb ceramics has a higher demand for computational resources. The differences in heat conduction, thermal stress, and computational efficiency of different materials indicate that the PINNs model can effectively adapt to the thermal environment of different biomaterials, and the simulation ability is stronger in the region of high temperature gradient and high stress concentration. Cellular ceramics are suitable for efficient thermal conductivity applications, but their high-temperature stress concentration problem requires further optimization of the structural design, whereas natural rubber and polymers exhibit better thermal buffering properties and are suitable for thermal insulation and thermal stress-resistant material application scenarios.

6. Optimization strategies for PINNs algorithm in 3D biomechanical heat transfer problems

a) Model Uncertainty Handling

In order to improve the predictive robustness of the model under high temperature gradient and non-uniform stress field, a Bayesian uncertainty estimation method is introduced. Specifically, the Monte Carlo Dropout (MCD) strategy is used, where the dropout is kept active during the training phase, and the set of outputs $\{\hat{y}_1, \hat{y}_2, \ldots, \hat{y}_T\}$ under the same input x is obtained through multiple forward propagations T times, and its mean $\mu = \frac{1}{T}\sum_{t=1}^{T} \hat{y}_t$ and variance $\sigma^2 = \frac{1}{T}\sum_{t=1}^{T}(\hat{y}_t - \mu)^2$ are computed, thus estimating the prediction uncertainty [15]. This method can

quantify the sensitivity to input perturbations through the neural network structure without explicitly defining the prior distribution. Meanwhile, in order to alleviate the problem of excessive error in high temperature gradient or stress concentration regions, the Adaptive Weighted Loss (AWL) mechanism is introduced. The overall loss function is defined as:

$$L_{total} = \sum_{i=1}^{N} w(x_i) \cdot \|F(x_i;\theta) - y_i\|^2 \tag{10}$$

where $w(x_i) + 1 + \alpha \cdot |\nabla T(x_i)|$ is the weight factor associated with the local temperature gradient and α is the tuning hyperparameter. This strategy enables the model to automatically give higher attention to high gradient regions during training, which helps to alleviate the problem of insufficient local convergence and improve the overall prediction accuracy. To enhance the practicality and scalability, a parallel GPU-based Monte Carlo Dropout sampling mechanism is incorporated into the computational process, and the dynamic adjustment of $w(x)$ enables intensive optimization training in high-temperature/high-stress regions. The method realizes the organic integration of uncertainty quantification and accuracy control in high-dimensional fields.

In order to optimize the computational stability, Multi-Scale Grid Sampling (MSGS) is used to increase the sampling density in the region where the temperature change is more than 500 K/m or the stress change is more than10^5 Pa/m, so as to make the computational accuracy in the region where the gradient changes are drastic. The loss function optimization adopts an adversarial training strategy to optimize the model's robustness by counteracting noise perturbations and to ensure the model's adaptability in large-scale biological tissues. In order to analyze the performance of PINNs in uncertainty optimization more intuitively, **Figure 5** shows the distribution of uncertainty in different regions, and the uncertainty heatmap on the right side shows that the uncertainty of PINNs is significantly reduced in high gradient regions.

$$L = \lambda_1 \left\| \frac{\partial T}{\partial t} - \nabla \cdot (k \nabla T) - \frac{q}{\rho c} \right\| + \lambda_2 \|\nabla \cdot \sigma - f\|^2 + \lambda_3 \|\mathrm{IE}[T] - T_{true}\|^2 \tag{11}$$

where $\mathrm{IE}[T]$ denotes the expected temperature distribution based on Bayesian uncertainty estimation, and λ_3 is the uncertainty correction weight, which ensures that the deviation between the predicted mean and the real data is minimized. The computational efficiency of Monte Carlo Dropout is improved to 10^6 forward propagation calculations per second by GPU parallel computing optimization, which improves the computational stability and accuracy of PINNs in complex biological tissue heat transfer problems.

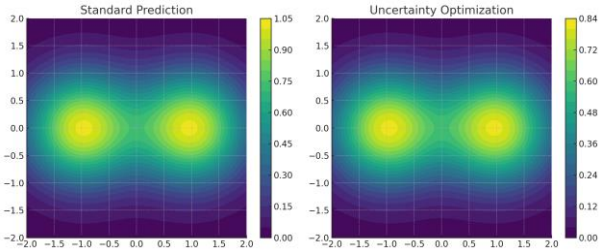

Figure 5. Heat map of uncertainty distribution.

b) Optimization of network structure and training strategy

In order to improve the accuracy and generalization ability of the PINN algorithm in 3D biomechanical heat transfer problems, the network structure is a 12- to 24-layer deep fully connected network (D-FCN) with 128 to 1024 neurons per layer, and the activation function is chosen to be Swish. The input variables include the 3D coordinates (x, y, z), the time t, and the material parameters (the thermal conductivity k is 0.1–10 W/m-K, density ρ of 500–1500 kg/m^3, and specific heat capacity c of 1000–4000 J/kg-K), and the outputs are the temperature field T and the stress distribution σ. The loss function combines the heat conduction and the constraints of the mechanical equations, the optimization method is L-BFGS with Adam, and the convergence error is controlled within 10^{-4}. The data sampling strategy uses adaptive grid refinement to increase the sampling density when the temperature gradient exceeds 500 K/m or the stress gradient exceeds 10^5 Pa/m; in the 300–350 K interval, the sampling density is encrypted to 5000/m^2. Adversarial Perturbation Optimization (APO) is introduced to simulate tissue nonuniformity by noise and construct the adversarial loss function Ladv. The nonuniformity of biological tissues is simulated by adding random noise to the input data and constructing the adversarial loss function L_{adv}:

$$L_{adv} = \lambda_4 \| \mathrm{IE}[T + \delta] - T_{true} \|^2 \tag{12}$$

where δ denotes the random perturbation term and λ_4 is used as the adversarial learning weight to enhance the model's adaptability to the complexity of real biological tissues. During the training process, the batch size is set to 4096 in the GPU parallel computing environment, and the optimization algorithm adopts a hybrid strategy, which first uses Adam for the first 10,000 times of training, with the learning rate set to 10^{-3}, and then switches to L-BFGS to enhance the global optimization capability. The parameters of the model are updated by gradient clipping, which restricts the gradient parameter to within 1.0 to avoid the gradient explosion phenomenon and improve the numerical stability of the model.

$$\theta_{t+1} = \theta_t - \eta \nabla L(\theta_t), where \| \nabla L(\theta_t) \| < 1.0 \tag{13}$$

During the optimization computation, to reduce computational overhead, Mixed Precision Training (MPT) is used, which uses FP16 precision for forward propagation and backpropagation computations while maintaining FP32 precision for gradient updates to reduce storage requirements and increase training speed. The computational task is based on NVIDIA RTX 3090 GPUs, and the parallel computational throughput is increased to 10^6 gradient updates per second. In order to analyze the effect of the optimization strategy more intuitively, **Figure 6** shows

the comparison of the loss convergence curves under different training strategies, and the right figure shows the data distribution after adaptive mesh optimization, which significantly reduces the error accumulation in the high-temperature gradient region.

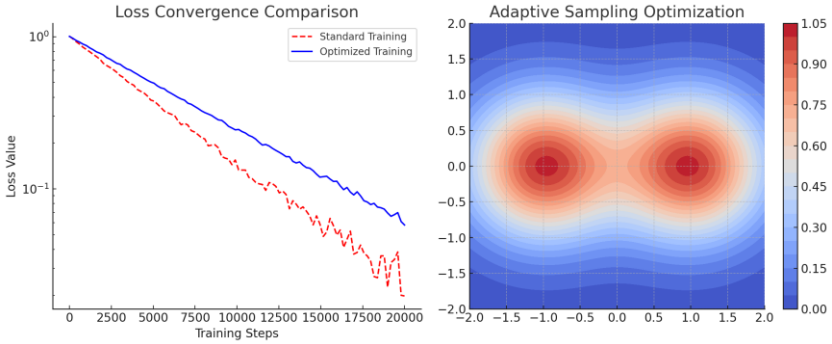

Figure 6. Comparison of loss convergence curves with different training strategies.

c) Physical constraint enhancement methods

The enhancement of physical constraints in the PINNs model for the 3D biomechanical heat transfer problem is optimized through several aspects. For the boundary conditions of the temperature and stress fields, an adaptive boundary processing method is used, which makes the model give higher computational accuracy in the region of high temperature gradient and stress concentration by dynamically adjusting the weights of the boundary terms in the loss function. In addition, a local weighting strategy is introduced to increase the density of training points in regions with large temperature and stress gradients, thus improving the prediction accuracy in these regions. During the training process, a gradient weighting technique is used to adjust the learning rate of different physical regions, enabling the model to capture changes in heat transfer and stress distribution more accurately in complex biomechanical environments. Through these enhancement methods, the model is able to effectively improve its adaptability to high-temperature regions, non-uniform materials, and complex boundary conditions, thus improving the overall prediction performance and numerical stability.

7. Conclusion

The application of the PINNs algorithm to 3D biomechanical heat transfer problems demonstrates strong numerical stability and prediction accuracy. By introducing physical constraints and combining them with the automatic differentiation technique, the model shows high accuracy in predicting the temperature and stress fields in complex biological tissues, especially in dealing with anisotropic, non-uniform, and heat-force coupling problems under complex boundary conditions. The experimental results show that the PINNs algorithm is effective in improving the numerical stability in high gradient regions, optimizing the stress distribution in complex geometric scenarios, and reinforcing the accurate fitting of temperature mutation regions. In the future, more complex physiological activity models can be further combined to introduce biothermodynamic factors such as blood perfusion and metabolic heat in order to enhance the model's ability to

portray the heat transfer behavior of real biological tissues. In addition, the combination of multi-scale grid optimization and adaptive sampling strategy will help to further improve the computational efficiency and applicability of the algorithm in large-scale biomechanical models.

Ethical approval: Not applicable.

Informed consent statement: Not applicable.

Conflict of interest: The author declares no conflict of interest.

References

1. Zhu J. Exploration of the application of thermal conductivity of bio-textile materials in wearable devices: Insights from molecular biomechanics within cells. Molecular & Cellular Biomechanics. 2025; 22(1): 504-504.
2. Bowden EE, Carter JD, Bowden AE, et al. Significant Environmental Factors in the Drift of Electrical Properties in Conductive Nano-Composite Sensors for Biomechanical Motion-Tracking. Journal of Biomedical Materials Research Part A. 2024; 113(1). doi: 10.1002/jbm.a.37863
3. Cai S, Wang Z, Wang S, et al. Physics-informed neural networks for heat transfer problems. Journal of Heat Transfer, 2021, 143(6): 060801.
4. Kim SU, Kim JY. Development of a Biomechanical Diagnosis and Analysis System Using a Textile Elbow Angle Sensor: Integrating Inverse Dynamics and Multi-Layer Perceptron Techniques. Processes. 2025; 13(3): 748. doi: 10.3390/pr13030748
5. Salem MG, Abouelregal AE, Elzayady ME, et al. Biomechanical response of skin tissue under ramp-type heating by incorporating a modified bioheat transfer model and the Atangana–Baleanu fractional operator. Acta Mechanica. 2024; 235(8): 5041-5060. doi: 10.1007/s00707-024-03988-x
6. Li R, Zhou J, Wang JX, et al. Physics-Informed Bayesian Neural Networks for Solving Phonon Boltzmann Transport Equation in Forward and Inverse Problems with Sparse and Noisy Data. ASME Journal of Heat and Mass Transfer, 2025, 147(3): 032501.
7. Kużdżał A, Muracki J, Makar P, et al. Assessment of the Impact of Heat-Compression Therapy Time on Muscle Biomechanical Properties and Forearm Tissue Perfusion in MMA Fighters—A Pilot Study. Applied Sciences. 2024; 14(19): 8659. doi: 10.3390/app14198659
8. Schmid QT, Ruschke S, Karampinos DC, et al. Development of a 3D-knee brace joint using MRI data and a genetic algorithm. Sports Engineering. 2025; 28(1). doi: 10.1007/s12283-025-00486-8
9. Gonçalves ND, de Sá Rodrigues J. Heat Conduction Control Using Deep Q-Learning Approach with Physics-Informed Neural Networks. Metrology. 2024; 4(3): 489-505. doi: 10.3390/metrology4030030
10. Shang Y, Tan C, Yu X, et al. Using neural networks: a guidance with application in inverse heat conduction problem. European Journal of Physics. 2025; 46(2): 025102. doi: 10.1088/1361-6404/ada741
11. Baldan M, Di Barba P. Energy-based PINNs for solving coupled field problems: Concepts and application to the multi-objective optimal design of an induction heater. IET Science, Measurement & Technology. 2024; 18(9): 514-523. doi: 10.1049/smt2.12212
12. Song Y, Yuan X, Yue H. The ADMM-PINNs Algorithmic Framework for Nonsmooth PDE-Constrained Optimization: A Deep Learning Approach. SIAM Journal on Scientific Computing. 2024; 46(6): C659-C687. doi: 10.1137/23m1566935
13. Kokash H, Khanafer K, Burzo M. Machine Learning-Based Predictions of Flow and Heat Transfer Characteristics in a Lid-Driven Cavity with a Rotating Cylinder. Energies. 2024; 17(20): 5220. doi: 10.3390/en17205220
14. Edalatifar M, Shafi J, Khalid M, et al. An artificial intelligence approach for the estimation of conduction heat transfer using deep neural networks. International Journal of Numerical Methods for Heat & Fluid Flow. 2024; 34(8): 3107-3130. doi: 10.1108/hff-11-2023-0678
15. Singhal M, Goyal K, Singla RK. A review of regularization strategies and solution techniques for ill-posed inverse problems, with application to inverse heat transfer problems. Reviews in Mathematical Physics. 2023; 36(01). doi: 10.1142/s0129055x23300078